

Binding of an oxide layer to a metal: the case of $\text{Ti}(10\bar{1}0)/\text{TiO}_2(100)$

Linggang Zhu,[†] Qing-Miao Hu,[‡] Rui Yang,[‡] and Graeme J. Ackland^{*,†}

*SUPA, School of Physics and Astronomy, The University of Edinburgh, Edinburgh EH9 3JZ, UK,
and Shenyang National Laboratory for Materials Science, Institute of Metal Research, Chinese
Academy of Sciences, Shenyang 110016, China*

E-mail: gjackland@ed.ac.uk

*To whom correspondence should be addressed

[†]SUPA, School of Physics and Astronomy, The University of Edinburgh, Edinburgh EH9 3JZ, UK

[‡]Shenyang National Laboratory for Materials Science, Institute of Metal Research, Chinese Academy of Sciences, Shenyang 110016, China

Abstract

We study the chemical nature of the bonding of an oxide layer to the parent metal. In order to disentangle chemical effects from strain/misfit, $\text{Ti}(10\bar{1}0)/\text{TiO}_2(100)$ interface has been chosen. We use the density functional pseudopotential method which gives good agreement with experiment for known properties of bulk and surface Ti and TiO_2 . Two geometries, a film-like model (with free surface in the structure) and a bulk-like model (with no free surface in the structure) are used to simulate the interface, in each case with different terminations of Ti and TiO_2 . For the single-oxygen interfaces, the interface energy obtained using these two models agree with each other; however for the double-oxygen ones, the relative stability is quite different. The disturbance to the electronic structure is confined within a few atomic layers of the interface. The interfacial bonding is mainly ionic, and surprisingly there is more charge transfer from Ti to O in the interface than in the bulk. In consequence the Ti/ TiO_2 interface has stronger binding than the bulk of either material. This helps to explain why the oxide forms a stable, protective layer on Ti and Ti alloys.

INTRODUCTION

In contrast to the many atomistic studies of metals and oxides, both at the ab initio and empirical level, the metal-oxide interface is much less well studied. This may appear surprising given its central role in corrosion. One reason may be the difficulty in identifying a candidate interface where the chemical effects are not entangled with misfit strain energy. Another is the relatively large size of system which is required to isolate the system. Although the strain energy is long-ranged, there are reasons to expect that the chemical effects of the interface may not be: on the metal side the free electrons should screen the Coulomb forces, while the image charges induced in the metal should mimic the electrostatics of a bulk oxide. At the interface itself, such classical ideas break down, and a full quantum treatment is needed to determine the nature of the bonding. In this paper we will consider the low-misfit $\text{Ti}(10\bar{1}0)/\text{TiO}_2(100)$ interface, with a view to determining the range over which chemical effects are significant and the nature of the bonding cross the interface.

Titanium alloys are widely used in many fields such as the aerospace industry, chemical plants, and even sporting goods. The high strength-to-weight ratio and excellent corrosion resistance account for its wide application. The corrosion property is mainly a result of the formation of stable protective oxide film, which consists primarily of TiO_2 . However, above 600°C , the fast diffusion of oxygen through the oxide layer into the bulk can result in excessive growth of oxide layer and embrittlement of the adjacent oxygen rich layer of the titanium alloy, which limits its maximum use temperature.¹ Alloying and coating have been found effective to address this problem. Obviously, the interface between the titanium and its oxide plays a vital role in the corrosion, both through its adhesive strength and the diffusion of species (O and/or Ti) through it, and its structure is a key aspect for understanding the behavior of titanium alloys.

Extensive experiments on pure titanium²⁻⁵ and titanium alloys^{6,7} have established that the crystal structure of the oxide is normally rutile (tetragonal, $P4_2/mnm$). Although Guleryuz et al.⁸ reported some diffraction angles consistent with the anatase structure (tetragonal, $I4_1/amd$), in the scale of Ti-6Al-4V oxidized at 600°C , rutile is the dominant oxide at 650°C . Due to the competition between surface free energy and strain energy, the growth of rutile on pure titanium exhibits a preferential direction,^{3,4} with a specific crystallographic orientation relationship (COR) between titanium and rutile. Three possible CORs between Ti and rutile were established by Flower et al.² using an *in situ* method: $\text{Ti}(0001)[11\bar{2}0] // \text{TiO}_2(010)[001]$, $\text{Ti}(10\bar{1}0)[0001] // \text{TiO}_2(100)[010]$ and $\text{Ti}(11\bar{2}0)[0001] // \text{TiO}_2(001)[100]$. Among these three different matchings, $\text{Ti}(10\bar{1}0)[0001] // \text{TiO}_2(100)[010]$ has the smallest mismatch on the plane of the interface, which means only a tiny interface strain would be required.

The structure of the oxide and the orientation relationship can be easily determined by the experiments; however, some other quantities like the chemical composition, atomic structure of the interface, and the nature of the bonding (ionic/metallic/covalent) across the interface are currently experimentally inaccessible. Fortunately, nowadays, it is possible to deal with coherent interface structures (large system, low symmetry) using accurate first-principles theoretical methods to obtain those quantities. Coherency implies that one part (metal or oxide) will be strained to match the

other one perfectly to maintain the coherency without misfit dislocations. In this case, DFT supercell method can be a good tool to study interfaces with small mismatch, but even when the misfit is quite big, it has been assumed that the interfacial regions between the misfit dislocation being modelled.⁹ Such a first-principles supercell method has been used to study many different interfaces, for example, interface of ZrO_2/Ni ,¹⁰ $\text{Al}/\text{Al}_2\text{O}_3$,⁹ Ti/TiN ,¹¹ $\text{YSZ}/\text{Al}_2\text{O}_3$,¹² $\text{Nb}/\text{Nb}_5\text{Si}_3$,¹³ etc. Here we present a DFT study of $\text{Ti}(10\bar{1}0)[0001] // \text{TiO}_2(100)[010]$ interface. The purpose of this study is to determine the optimal atomic structure and energy of $\text{Ti}(10\bar{1}0)[0001] // \text{TiO}_2(100)[010]$ interface, and characterize the nature of the interfacial bonding.

METHODS

The Vienna Ab initio Simulation Package (VASP)^{14–16} utilizing a plane-wave basis set for the expansion of the single-particle Kohn-Sham wave functions, was used in this study. The projector augmented wave (PAW) method,¹⁷ was employed to describe the electron-core interaction. The $3p$ semicore electrons of Ti were treated as valence, given a 10-electron PAW-pseudopotential. For the exchange-correlation interaction, we adopted generalized gradient approximation (GGA) as parameterized by Perdew and Wang (PW91).¹⁸ A high cutoff energy of 525 eV was used. Sampling of the Brillouin zone was performed with a Monkhorst-Pack grid.¹⁹ Ground-state atomic structures were obtained by minimizing the Hellmann-Feynman forces on the atoms, and all the atoms were free to relax. The relaxations terminate when the maximum force on the atoms is less than 0.05 eV/Å. For some calculations a dipole moment is present, in such cases the divergent terms are removed by the Ewald sum; we did not include a dipole correction[?] as previous work in TiO_2 has shown this to have minor effects.

Table 1: Structure parameters (internal coordinate u in TiO_2 refers to the position of the oxygen atom in the unit cell), bulk modulus B_0 (GPa), compared with experimental data.

	HCP-Ti			TiO ₂			
	a(Å)	c(Å)	B_0	a(Å)	c(Å)	u	B_0
This work.	2.934	4.638	115	4.645	2.971	0.305	206
Expt. ^a	2.951	4.674	110	4.587	2.954	0.305	216

^a Data for Ti and TiO₂ are from refs 20 and 21

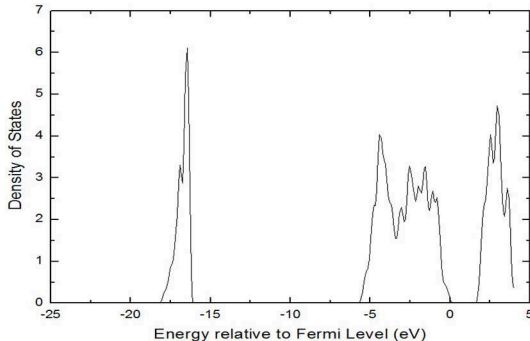


Figure 1: DOS per TiO₂ unit in bulk rutile.

RESULTS: parameters and basic properties of Ti and TiO₂

Bulk properties

To verify the accuracy of our computational parameters, we first calculated the bulk properties of Ti and rutile. The k-point mesh was set at $5 \times 5 \times 8$ and $11 \times 11 \times 7$ for the bulk TiO₂ and hcp-Ti, respectively. These provide convergence to within 1 meV and as can be seen from 1 the calculated lattice parameter and bulk modulus data agree excellently with the experiments. From the DOS of TiO₂ (1), the gap between highest occupied and lowest unoccupied state of TiO₂ is about 1.7 eV, far away from the experimental value, which is around 3.0 eV:²² this does not affect the bonding and is typical of the error of DFT in describing excited states.

Surface properties

To determine the minimum slab thickness needed to reliably calculate the surface/interface we examined the convergence of the relaxation and energy of the surfaces with respect to slab thickness. In this calculation, we used k-point sampling $8 \times 5 \times 1$ and $5 \times 8 \times 1$ for Ti(10 $\bar{1}$ 0) and TiO₂(100).

In both slabs, a 15 Å vacuum region is introduced to avoid the interaction between periodic images. For both surfaces, only the (1 × 1) structures (along the two lattice vectors of the surface, the symmetry is the same as in the bulk) are considered, since these have been observed by for clean surface under normal conditions by experimentalists.^{23–25}

The calculated surface energy might diverge with the thickness of the slab, if there is any numerical difference between the calculation of bulk and slab, arising, for example, from the k-point mesh. Following Boettger²⁶ we avoid this possibility, by evaluating the surface energy γ as follows:

$$\gamma = (E_{\text{slab}}^N - N\Delta E_{\text{slab}}^{N'} / \Delta N) / 2S \quad (1)$$

$$\Delta E_{\text{slab}}^{N'} = E_{\text{slab}}^{N'} - E_{\text{slab}}^{N'-\Delta N}$$

where N' is the minimum number of the slab layers for which the energy converges, E_{slab}^N is the energy of a N -layer slab, and S is the area of the surface.

Ti(10 $\bar{1}$ 0)

In hcp Ti, two different (10 $\bar{1}$ 0) planes exist, depending on whether the surface terminates in a large (1.694 Å) or small (0.847 Å) interlayer spacing. From the experimental results,²⁴ Ti(10 $\bar{1}$ 0) surface with a small first interlayer spacing was the favored one. Our calculation confirmed this, and henceforth, we concentrate on the more stable Ti(10 $\bar{1}$ 0) surface.

Table 2: Interlayer distance relaxation of the Ti(10 $\bar{1}$ 0) surface vs slab thickness, shown as a percentage of the bulk spacing. The surface energy γ obtained with different slab thickness is also listed, in J/m².

Layer	Δd_{12}	Δd_{23}	Δd_{34}	Δd_{45}	Δd_{56}	Δd_{78}	Δd_{89}	γ
12	-3.26	-5.43	5.98	-2.20	3.65			1.99
14	-3.64	-4.74	4.10	-1.13	2.19	2.16		1.99
16	-3.75	-4.80	3.95	-1.01	1.97	1.25	-0.29	1.99
18	-3.70	-4.93	3.99	-1.18	2.07	1.39	-0.39	1.99
Expt. ^a	-5.9							

^a ref24

The surface relaxation data is shown in 2, the distance between the first two layers d_{12} decreases by about 4% compared with that in the bulk, in reasonable agreement with 6% from the experiment²⁴ (the discrepancy is less than 0.02 Å). d_{23} contracts and d_{34} expands, showing the same trend as the results by self-consistent tight bonding model.²⁷ Relaxations between deeper layers are even smaller (less than 2%). The surface energy converged quickly with cell size to 1.99 J/m². This is slightly higher than the 1.91 J/m² of Ti(0001) surface which we obtained using the same method: Ti(0001) has an experimental energy of 1.99 J/m².²⁸ Thus Ti(10 $\bar{1}$ 0) is just slightly less stable than the close-packed Ti(0001) surface. For further study, we chose a 16-layer slab to simulate Ti(10 $\bar{1}$ 0).

TiO₂(100)

Extensive theoretical studies have been done to investigate the TiO₂(100) surfaces. There are three possible terminations for TiO₂(100), which we call O-Ti-O, O-O-Ti, and Ti-O-O (named by the atomic arrangement from the surface to inner layer). The first of these (2) has the smallest surface polarization due to the symmetrical arrangement of O, and the geometry has been observed by experiment.²⁵ We find it to be the most stable one, and we use the O-Ti-O terminated TiO₂(100) surface to determine the minimum thickness of the slab needed. One thing that should be noted is that in this subsection, the O-Ti-O unit is treated as one layer, i.e., the 5-layer slab mentioned here has 15 atomic layers.

The choice of exchange-correlation functional has been found to affect the surface energy quite significantly,²⁹ and normally LDA gives a higher surface energy than GGA. Due to the lack of the experimental results, it is difficult to clarify which function best describes the real situation. Here, we compared our results with other calculations using the same exchange-correlation function (GGA), in order to verify the accuracy of our calculation. As shown in 3, O₁, Ti₂, and O₃ exhibit large relaxations along [0 $\bar{1}$ 0]. Moreover, Ti₂ relaxes inward along [100], while outward relaxation is observed for O₁ and O₃. These relaxations increase the effective coordination of Ti₂ (fivefold).^{29,30} Our surface relaxation results agree with that found by Muscat et al..²⁹ 4 lists the

surface energy dependence on the slab thickness: it converges quickly to 0.68 J/m^2 which agrees very well with Perron et al.³¹ (10 valence electrons are considered for Ti) and Labat et al. (GGA-PBE),³⁰ while it is smaller than Muscat’s GGA result.²⁹ Considering the convergence of both the surface structure and energy, we believe that a 13-layer slab is thick enough to model $\text{TiO}_2(100)$.

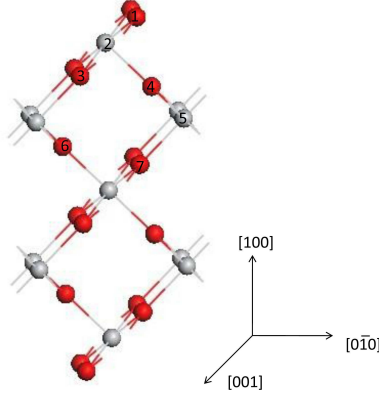


Figure 2: $\text{TiO}_2(100)$ surface structure. Red spheres represent O atoms, and silver spheres represent Ti atoms.

Table 3: The displacement of ions (\AA) (as labeled in 2) relative to the bulk terminated structure of $\text{TiO}_2(100)$ surface obtained with different slab thickness.

Label	5		9		13		17		Ref. ^a	
	$[0\bar{1}0]$	$[100]$	$[0\bar{1}0]$	$[100]$	$[0\bar{1}0]$	$[100]$	$[0\bar{1}0]$	$[100]$	$[0\bar{1}0]$	$[100]$
1	0.32	0.07	0.32	0.08	0.28	0.06	0.28	0.06	0.31	0.06
2	-0.10	-0.03	-0.11	-0.02	-0.15	-0.03	-0.15	-0.03	-0.11	-0.04
3	0.17	0.06	0.18	0.08	0.14	0.06	0.13	0.05	0.13	0.02
4	0.07	0.01	0.08	0.02	0.04	0.01	0.04	0.00	0.03	0.00
5	-0.05	0.02	-0.06	0.04	-0.10	0.03	-0.10	0.02		
6	0.01	0.03	0.04	0.04	0.00	0.02	0.00	0.02		
7	0.01	-0.01	0.04	0.01	0.01	-0.01	0.01	-0.01		

^aref29.

Table 4: The dependence of surface energy of $\text{TiO}_2(100)$ on slab thickness, in unit of J/m^2 .

Layer	5	9	13	17	Ref. ^a	Ref. ^b	Ref. ^c
γ	0.70	0.68	0.68	0.68	0.67	0.69	0.83

^a ref 31; ^b ref 30; ^c ref 29.

RESULTS: Interface properties

The orientation relationship is set as $\text{Ti}(10\bar{1}0)[0001] // \text{TiO}_2(100)[010]$ across the interface. The size of the $\text{Ti}(10\bar{1}0)$ surface cell is $2.934 \text{ \AA} \times 4.638 \text{ \AA}$, while it is $2.971 \text{ \AA} \times 4.645 \text{ \AA}$ for $\text{TiO}_2(100)$. A coherent interface is obtained by a small strain of the softer Ti to perfectly match the $\text{TiO}_2(100)$ surface cell: this has little effect on the energy since the mismatch of the two surface cells is so small. To check dependence on boundary conditions we used two models to simulate the interface, a film-like model with an interface and two free surfaces, and a bulk-like model with two interfaces. The interface structures were relaxed with k-point mesh $3 \times 3 \times 1$ (four irreducible k points).

Film-like interface model

The film-like model is generated with 16-layers of Ti, 13-layers of TiO_2 and a 15 \AA vacuum region. This gives one interface and two free surfaces.

Various terminations of the surfaces and metal/oxide interface are possible, their stability depending on the environmental condition like the partial pressure of O_2 gas.³² As we mentioned above, $\text{TiO}_2(100)$ has three possible terminations, with uppermost layers O-O-Ti, O-Ti-O, and Ti-O-O. For interfaces, we considered different stacking sequences of Ti onto these terminations. Following work on other interfaces,^{9,11} the first layer of the Ti-metal is placed...

- 'OT': directly above uppermost Ti cations;
- 'HCP': above the second layer of Ti cations;
- 'FCC': above the third layer of Ti cations.
- 'TT': for O-O-Ti, as an extension of the oxide.
- 'TT': for Ti-O-O, as an extension of the metal.

The 'TT' configurations are those which would allow growth of the oxide/metal by simple extension of a stable interface, with the Ti 'atoms' and Ti 'cations' directly adjacent. In fact, the

two 'TT' configurations are the same at the interface, the calculation differing in the accompanying surface.

Despite this apparently exhaustive survey of stacking sequences, we also found that where the TiO₂(100) surface is quite corrugated, significant reconstruction can occur within the Ti-metal region, spontaneously generating a stacking fault. When this happens, we report the most stable relaxed structure, and label it 'HCP-2' and 'FCC-2' in 5.

To avoid spurious contraction due to surface tension, we fix the lattice parameters in the interface plane. But we allow relaxation perpendicular by first calculating the total energy of the unrelaxed interface structure as a function of interface separations d . Once the optimal value is found, all the atoms are relaxed to the ground state at fixed volume.

In order to evaluate the strength of the interface, we calculated the work of adhesion, W_{ad} , which is defined as:

$$W_{ad} = (E_M^{\text{tot}} + E_O^{\text{tot}} - E_{M/O}^{\text{tot}})/S$$

where E_M^{tot} is the surface energy of Ti-metal, E_O^{tot} is the surface energy of oxide, $E_{M/O}^{\text{tot}}$ is the energy of the interface structure, and S is the interface area. A positive value of W_{ad} means that the interface is energetically favorable over the free surfaces. 5 shows that W_{ad} increases with increasing number of interfacial O atoms (Ti-O-O, O-Ti-O, and O-O-Ti). However, much of this is due to differences in surface stability; e.g. the O-O-Ti and Ti-O-O with 'TT' stacking have the same chemical composition near the interface but very different W_{ad} .

To understand the growth of an additional TiO₂ layer, each of these interface types needs to be considered. In the following subsections, the interface with the most stable stacking sequence for each termination is analyzed in detail.

For all configurations listed in 6, for the metal slab, the Ti atom in the center has a charge 0.00, as in bulk Ti, which again confirms that the slab we used is thick enough. For the TiO₂ slab, the charge associated with central Ti and O ions are $2.18e$ and $-1.10e$, respectively. This agrees well with DFT+ U results from Jess and the co-workers³³ who found the Bader charge is $2.22e$ and

Table 5: Relaxed values of W_{ad} (J/m^2) for interfaces with different termination and stacking sequence, with interfacial distance d (\AA).

	O-O-Ti					O-Ti-O				Ti-O-O			
	OT	HCP	FCC	TT	HCP-2	OT	HCP	FCC	FCC-2	OT	HCP	FCC	TT
d	1.65	0.57	1.09	0.97	1.17	1.87	1.37	0.33	0.31	1.90	1.66	1.58	0.55
W_{ad}	7.54	9.43	8.99	9.32	10.34	2.28	2.57	3.49	3.55	1.41	2.59	2.04	2.83

$-1.12e$ for Ti and O. Although Bader charge values are far from the formal charge $4e$ (Ti^{4+}) and $-2e$ (O^{2-}), we believe that useful bonding information can be obtained from the charge transfer.

Atomic, electronic structure of O-O-Ti interface

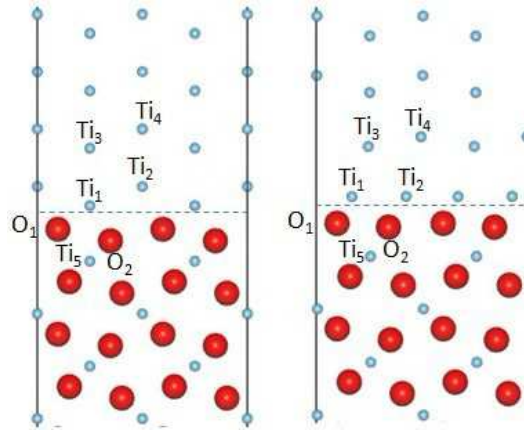


Figure 3: 'HCP-2' structure of O-O-Ti interface (only some layers near the interface is shown), viewed along $[001]$ direction of TiO_2 , the dashed line indicates the position of the interface. Left: without atomic relaxation (the equivalent atoms on the boundary are also shown). Right: with atomic relaxation. Large red spheres are O atoms, and small silver spheres are Ti atoms.

The stacking sequence 'HCP-2' gives rise to the most stable O-O-Ti interface (5). The structure is displayed in 3. To observe the geometry change due to the atomic relaxation clearly, the unrelaxed (input) structure is also shown and the ions with large displacement are labeled. On the metallic side, Ti_2 and Ti_4 move towards the oxide. Ti_1 and Ti_2 are found shifting along $[000\bar{1}]$ of Ti significantly. As a result, the surface morphology of $\text{Ti}(10\bar{1}0)$ is totally changed: the Ti_1 and Ti_2 layers merge to give a flat surface; the spacing between Ti_2 and Ti_3 layer changes to 2.19 \AA from 1.69 \AA in the bulk; the interlayer spacing between Ti_3 and Ti_4 decreases to 0.43 \AA from the bulk spacing 0.85 \AA . For the oxide slab, the relaxation is less significant, the interfacial atoms

move towards metal slab, in particularly O₂, thus the surface of the oxide becomes flatter. Across the interface, the separations of Ti₁-O₁ and Ti₂-O₂ is 2.00 Å and 2.15 Å, which is close to the Ti-O bond lengths in bulk TiO₂ (1.96 Å and 2.00 Å). O₂ is located in the center of the 'half' octahedron (formed by Ti₁, Ti₂ and Ti₅), and O₁ sits in a similar octahedral site.

Bader charge analysis³⁴ is applied to study the charge transfer. In 6, we give the Bader charge associated with the labeled atoms (3) as well as the atoms in the center of the metal/oxide slabs, and the value of the charge is the variation from the neutral Ti/O atom (10e for Ti, and 6e for O). Thus a negative value means accepting negatively charged electrons, while a positive value means donating electrons.

Table 6: Bader charge (*e*) of the selected atoms in the various interface structures (denoted by the termination, the model used, and the staking sequence in the bracket). Definitions of the atoms are given in the appropriate figures. Bulk values for Bader charge are 0.00 in Ti, and 2.18e and -1.10e for Ti and O in bulk rutile. For all the structures listed in the table, the Ti atom/ion in the center of the slab has the same Bader charge as in the bulk.

Atom	Ti slab				TiO ₂ slab			
	Ti ₁	Ti ₂	Ti ₃	Ti ₄	Ti ₅	O ₁	O ₂	O(center)
O-O-Ti film(HCP-2)	0.81	0.82	-0.21	0.32	2.08	-1.20	-1.28	-1.11
O-Ti-O film(FCC-2)	0.82	0.06	0.24	0.01	1.78	-1.37	-1.24	-1.10
Ti-O-O film(TT)	0.56	-0.06	0.18	-0.04	1.12	-1.27	-1.20	-1.09
S-O ^a bulk(FCC)	0.77	0.15	0.23	-0.09	1.78	-1.39	-1.24	-1.11
D-O ^b symmetry bulk(TT)	1.05	0.62	-0.01	0.12	2.10	-1.21	-1.27	-1.11
D-O ^b asymmetry bulk(TT)	1.06	0.60	-0.05	0.15	2.11	-1.27	-1.21	-1.11
D-O ^b asymmetry bulk(HCP-2)	0.83	0.81	-0.19	0.31	2.08	-1.19	-1.28	-1.11

^a Single-Oxygen; ^b Double-oxygen.

For 'HCP-2' each of the interfacial atoms Ti₁ and Ti₂ donates 0.8 electrons, which account for the net charge transfer of 1.61 electrons from the metal slab to the oxide (6). Bader analysis gives a negative charge for Ti₃, but this appears to be an artifact due to the large relaxation around it, leading to a large Bader volume, which in turn encloses more electrons. It is better to consider the layer containing Ti₃ and Ti₄, which has overall a small positive charge. The interfacial oxygen ions O₁ and O₂ attract more electronic charge than the oxygen in the center, due to the more electron donors nearby. Ti₅ transfers fewer electrons than the Ti ions in the center of the oxide, which is also understandable as its coordination is smaller. The large electron transfer found here implies

strong ionic bonding across the interface.

The electronic density of states is projected onto selected atoms to determine the bonding character (4). Notably, Ti_3 and Ti_4 are dissimilar, as is reflected in the peak/valley just below the Fermi level. The interfacial atoms Ti_1 and Ti_2 show a small hybridization peak in the region from -7.5 eV to -2.5 eV, representing weak covalent bonding to the oxygen nearby. Strong hybridization between the Ti $3d$ and O $2p$ is observed from the DOS of all ions on the TiO_2 side of the interface, indicating some covalent bonding in rutile.³⁵ Ti_5 has almost no Ti conduction band density: which implies that bonding in the O-O-Ti structure is not metallic. The DOS of O_1 and O_2 are similar to the oxygen in the center of oxide slab, with a small shift of both s and p peaks to a lower energy level indicating a stronger Madelung field at the interface, which can stabilize the system.³⁶ For the oxygen on the surface, the s orbital shows no shift, and the width of its p orbital is reduced. By comparing the total DOS of the interface slab (5(a)) and DOS of pure TiO_2 (1), we see a small peak around -7.5 eV induced by the interface atoms. This will be discussed further later.

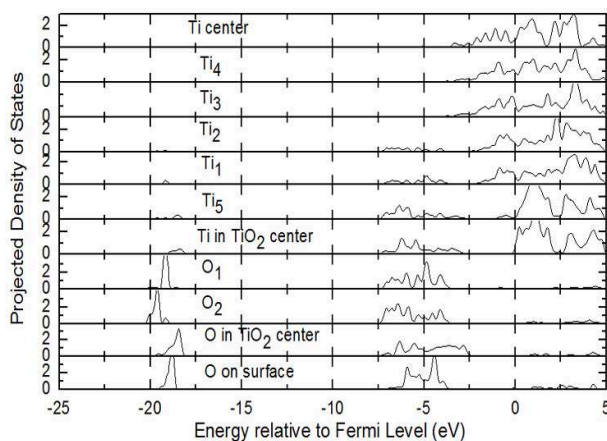


Figure 4: DOS projected onto selected atoms for the O-O-Ti interface. The labels of the atoms are identified in 3. Note that within TiO_2 all the states corresponding to the $4s3d$ band are unoccupied, consistent with formal ionic charges of Ti^{4+} and O^{2-} .

Atomic, electronic structure of O-Ti-O interface

As shown in 5, for O-Ti-O interface systems, the interface with strongest adhesion is 'FCC-2', which has a similar structure to 'FCC'. 6 shows the optimized 'FCC-2' interface: Ti_1 and Ti_3

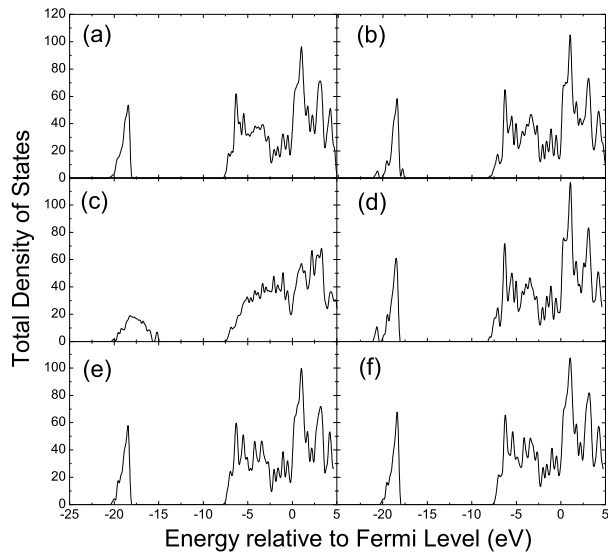


Figure 5: Total DOS of various interfaces using two models. (a) Total DOS of the O-O-Ti terminated interface using film-like model. (b) Total DOS of the O-Ti-O terminated interface using film-like model. (c) Total DOS of the Ti-O-O terminated interface using film-like model. In this interface slab, a O-O-Ti terminated $\text{TiO}_2(100)$ free surface is included. This polarized surface might account for the abnormal shape of the 2s states of oxygen. (d) Total DOS of the single-oxygen interface using bulk-like model. (e) Total DOS of the double-oxygen interface using symmetric structure of bulk-like model (including two 'TT' stacking interfaces). (f) Total DOS of the double-oxygen interface using asymmetric structure of bulk-like model (including one 'TT' and one 'HCP-2' stacking interface).

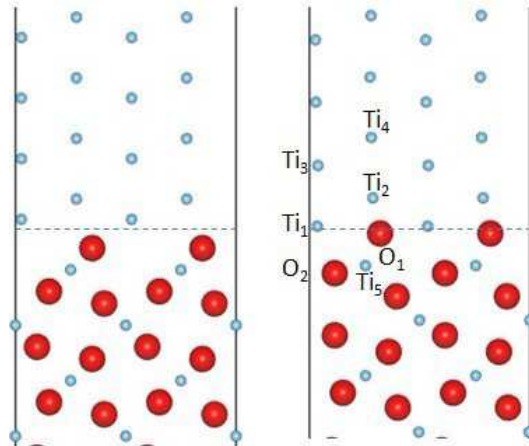


Figure 6: 'FCC-2' structure of O-Ti-O interface (only several layers near the interface is shown), viewed along [001] direction of TiO_2 , the dashed line indicate the position of the interface. Left: without atomic relaxation (the equivalent atoms on the boundary are also shown). Right: with atomic relaxation. Red spheres are O atoms, and silver spheres are Ti atoms.

are shifted significantly toward the oxide, forming planes containing both Ti and O atoms. With this displacement, the interlayer spacing of the metal slab near the interface changed to 1.19 Å and 1.36 Å, which are 0.85 Å and 1.69 Å in the bulk Ti, respectively. Relaxation of O₁ and O₂ leads to a displacement towards the metal even larger than that in the free surface structure. Finally, the separation O₁-Ti₂ and O₂-Ti₁ is 2.13 Å and 2.10 Å, close to the spacing in bulk TiO₂ (1.96/2.00 Å).

The Bader charge analysis results are listed in 6. The most significant charge transfer comes from Ti₁ and Ti₃, which donate a total of 1.16 electrons from the metal to the oxide. The excess charge is located on the interfacial atoms (Ti₅, O₁ and O₂).

As seen from 7, the atom-projected DOS converges rapidly to bulklike values away from the interface. For the interfacial ion Ti₅, states in the band gap of the oxide implies a kind of metallic behavior, and it is a little stronger than that in O-O-Ti interface, because of its direct exposure to the metal slab. The shift of DOS is very apparent in the interfacial atoms O₁ and O₂, especially for O₁, the 2s states is below -20 eV. For the surface oxygen, the 2s and 2p orbitals move to a higher energy level, which contribute to the small peak near -17.5 eV in the total DOS (5(b)). Also, comparing 1 (pure TiO₂), 5(b) (interface with surface), and 5(d) (interface with no surface), it can be concluded that, in 5(b), the small peak below -20 eV and peak near -7.5 eV are associated with the interface atoms, while the peak near -17.5 eV comes from surface atoms. These agree with the our calculation results that the formation of the interface is exothermic, while that is endothermic for the surface.

Atomic, electronic structure of Ti-O-O interface

For the Ti-O-O structures, 'TT' stacking exhibits the lowest energy. The input and relaxed structure of 'TT' stacking are shown in 8. Again, the relaxation tends to flatten the surfaces. The interfacial spacing (distance between Ti₁ layer and Ti₅ layer) is 0.55 Å, smaller than the 0.85 Å of the interlayer spacing in bulk Ti. O₁ moves towards the interface, which increases the effective coordination of Ti₅. The downward shift of Ti₁ and Ti₃ are also observed. The interlayer spacing

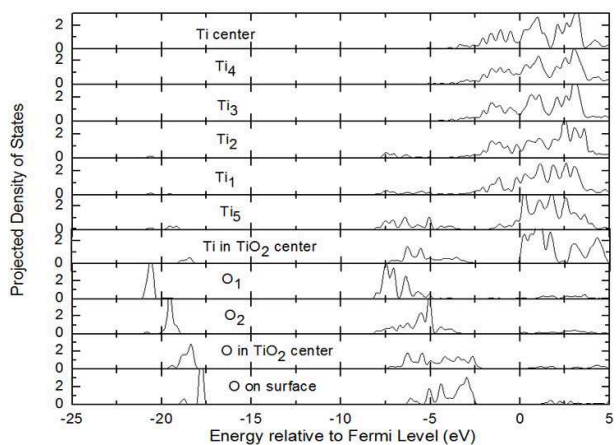


Figure 7: DOS projected onto selected atoms for the O-Ti-O interface. The label of the atom is identified in 6.

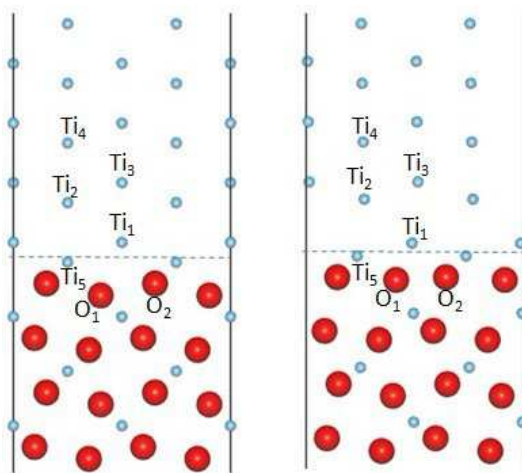


Figure 8: 'TT' structure of Ti-O-O interface (only several layers near the interface is shown), viewed along [001] direction of TiO_2 , the dashed line indicate the position of the interface. Left: without atomic relaxation (the equivalent atoms on the boundary are also shown). Right: with atomic relaxation. Red spheres are O atoms, and silver spheres are Ti atoms.

of $\text{Ti}_1\text{-Ti}_2$ and $\text{Ti}_2\text{-Ti}_3$ is 1.88 \AA and 0.74 \AA , respectively, which slightly deviate from the spacing in the bulk Ti.

The Bader charge analysis (6) and DOS projection (9) are qualitatively similar to the two systems. However, only $0.41e$ is moved to the oxide slab from the metal, much less than in the other two surfaces. From the projected DOS of the interfacial ions ($\text{Ti}_1, \text{Ti}_2, \text{Ti}_3$ and Ti_4), no covalent features are evident between the two slabs, but metallic bonding can be inferred from the occupied $4s3d$ states in Ti_5 which is adjacent to the metal slab. The relatively small W_{ad} of the Ti-O-O systems can be understood by the pDOS (9), where the $2s$ states of surface oxygen move to a very high level just below -15 eV . Thus the states between -15 eV and -17.5 eV in the 5(c) come from the oxygen near the free surface (O-O-Ti terminated) included in the slab model.

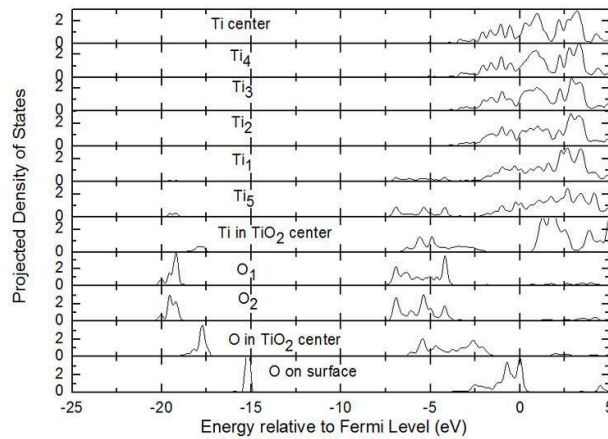


Figure 9: DOS projected onto selected atoms for the Ti-O-O interface. The label of the atom is identified in 8.

Bulk-like interface model

In this model, we consider a periodic arrangement $\cdots \text{metal-oxide-metal} \cdots$, with no free surfaces. One advantage of this model over the previous one is that the effects of surface dipole interactions are eliminated.

Considering the termination of $\text{TiO}_2(100)$ at the interface, there are two structures with different layer ordering

- $\cdots \text{Ti-Ti-Ti-O-Ti-O-O-Ti} \cdots \text{O-O-Ti-O-Ti-Ti-Ti} \cdots$,
- $\cdots \text{Ti-Ti-Ti-O-O-Ti-O-O-Ti} \cdots \text{O-O-Ti-O-O-Ti-Ti-Ti} \cdots$.

The former, denoted as *single-oxygen interface*, may have either two identical interfaces or different stacking sequences. For the latter, *double-oxygen interface*, we first calculate a 'TT' configuration where the first cation (metal) layer is like the extension of the metal (oxide). Subsequently we made an 'asymmetric' structure: one interface with 'TT' stacking, the other with 'HCP-2' stacking, so that the energy of the double-oxygen interface with 'HCP-2' stacking can be obtained. Again, we fix the dimensions of the cell in the interface plane.

In order to evaluate the strength of the interface, we defined the interface energy W_{bulk} as:

$$W_{bulk} = (E_{\text{Ti}m\text{O}n}^{\text{int}} - \frac{1}{2}E_{\text{TiO}_2}^{\text{bulk}} - (m - \frac{n}{2})E_{\text{Ti}}^{\text{bulk}}) / 2S$$

where $E_{\text{Ti}m\text{O}n}^{\text{int}}$ is the energy of interface structure consisting of m Ti atoms and n O atoms. $E_{\text{TiO}_2}^{\text{bulk}}$ is the energy per TiO_2 unit in the bulk oxide, $E_{\text{Ti}}^{\text{bulk}}$ is the energy per Ti atom in the bulk metal, and $2S$ is the area of the two interfaces in the interface structure.

The results are summarized in 8. The negative values indicate that the interface is favored relative to the bulk. In contrast to the results for the O-O-Ti terminated interface shown in 5, 'HCP-2' stacking here is less stable than the 'TT' stacking by about 0.1 J/m^2 .

To illustrate the possible effect of the free surface on the W_{ad} obtained by the film-like model, in 10, we display the structure of the Ti-O-O free surface from the film-like interface slab with 'TT' and 'HCP-2' stacking, compared with its structure in the pure $\text{TiO}_2(100)$ calculation. After relaxation in the surface slab (10(b)), O_1 and O_2 move significantly outwards, and finally, the Ti-O-O termination transforms to an arrangement like O-Ti-O. In TiO_2 , the surface terminated with Ti is highly polar and this outward movement of oxygen can decrease the dipolar moment. Very similar relaxation is observed in the interface with 'HCP-2' stacking (10(d)). However, for the 'TT' stacking (10(c)), the relaxation of O_1 and O_2 , does not occur, and the termination remains Ti-O-O. As we mentioned above, in 'TT' stacking, the first Ti layer of the metal sits in a position like

the extension of the oxide, so the O-O-Ti terminated interface with a stoichiometric oxide can also be seen as a Ti-O-O terminated interface with a non-stoichiometric oxide. This different surface relaxation directly affects the work of adhesion of the interface. We do not think this kind of interaction between the interface and polarized surface can be removed by increasing the thickness of the oxide slab.

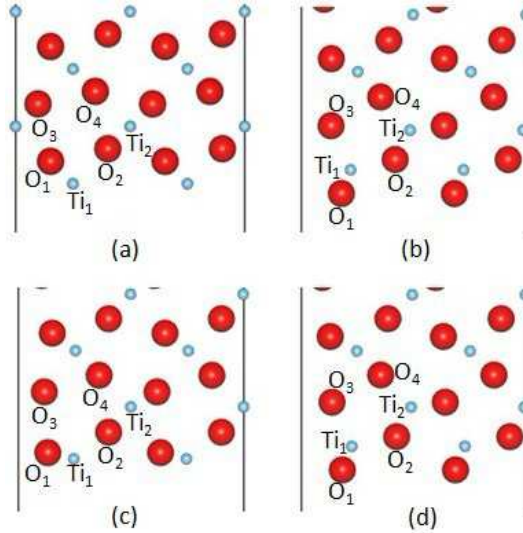


Figure 10: Structure of the Ti-O-O terminated TiO₂(100) surface. (a) unrelaxed structure (bulk termination), (b) relaxed structure in the TiO₂(100) surface slab, (c) relaxed structure in the O-O-Ti terminated interface slab with 'TT' stacking, (d) relaxed structure in the O-O-Ti terminated interface slab with 'HCP-2' stacking. Red spheres are O atoms, and silver spheres are Ti atoms.

Table 7: Bader charge (e) of the selected atoms on Ti-O-O surface included in different structures, the labels of the atoms are identified in 10(b), (c), and (d). Bulk values for Bader charge $2.18e$ and $-1.10e$ for Ti and O in bulk rutile.

Atom	surface TiO ₂ unit			inside TiO ₂ unit		
	Ti ₁	O ₁	O ₂	Ti ₂	O ₃	O ₄
free surface	1.94	-1.03	-1.19	1.88	-1.23	-1.13
TT stacking	1.56	-1.20	-1.16	2.11	-1.14	-1.10
HCP-2 stacking	1.93	-1.04	-1.19	1.88	-1.25	-1.14

In order to analyze the effects of interfaces on the Ti-O-O surface in detail, we examine the Bader charge on the ions near the surface in 7. In all cases the electron density near the surface is enhanced by almost one electron per surface cell. The charge distribution near the free surface is unaffected by an 'HCP-2' interface, but the presence of a 'TT' interface, changes the surface

charge distribution significantly. This interaction between surface and interface cast doubt on the validity of the film-like model. Similar calculations for the single-oxygen structures (terminated with O-Ti-O), show no such structure or Bader charge variation. Thus for the double-oxygen interface, the film-like model is still reliable.

So get an estimate of finite size error, we can directly compare the calculated work of adhesion for the same interface obtained by bulk-like and film-like calculation (5), and this requires subtraction of the energy of the free surfaces. These are: 1.99 J/m² and 2.20 J/m² for Ti(10 $\bar{1}$ 0) terminated with small and large interlayer spacing respectively; 0.68 J/m² for TiO₂(100) terminated with O-Ti-O, and 7.91 J/m² for the sum of Ti-O-O and O-O-Ti terminations. The resultant interface energy W_{film} is listed in 8. For the single-oxygen interfaces, W_{bulk} is in reasonable agreement with W_{film} . For the double-oxygen interface with 'TT' stacking the apparent discrepancy is obviously due to the different surface reconstruction, as just described. And the bulk-like model is more reasonable. In the next subsections, we will discuss the geometry as well as the electronic structure difference for these two models.

Table 8: Relaxed values for W_{bulk} (J/m²), compared with W_{film} that obtained by excluding the contribution of the surface energy from the work of adhesion by the film-like model.

Termination Stacking	single-oxygen				double-oxygen	
	OT	HCP	FCC	FCC-2	TT	HCP-2
W_{bulk}	0.30	-0.03	-0.95	-0.93	-0.60	-0.51
W_{film}	0.39	0.10	-0.82	-0.88	-0.05	

Atomic, electronic structure of single-oxygen interface

The structure of 'FCC' (11) is quite similar as the 'FCC-2' (6), in particularly the configuration near the interface and relaxations of the interfacial atoms (Ti₁, Ti₃, O₁, O₂) in the relaxed structure. Atom spacing O₁-Ti₂ and O₂-Ti₁ is 2.10 Å and 2.12 Å, very close to the results in 'FCC-2' stacking obtained by the film-like model, the Bader charge (6) and projected DOS on the interfacial atoms (12) are also similar to the film-like model. For the total DOS (5(d)), the surface-atom-induced small peak around -17.5 eV is absent, which is expected.

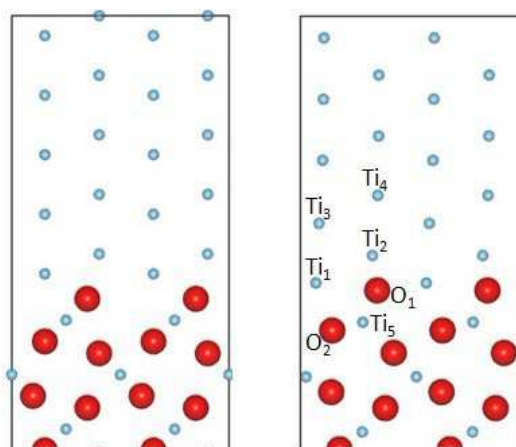


Figure 11: Structure of single-oxygen interface with 'FCC' stacking, viewed along [001] direction of TiO_2 . Only layers near one interface are shown: the other is symmetrically equivalent. Left: without atomic relaxation (the equivalent atoms on the boundary are also shown). Right: with atomic relaxation. Red spheres are O atoms, and silver spheres are Ti atoms.

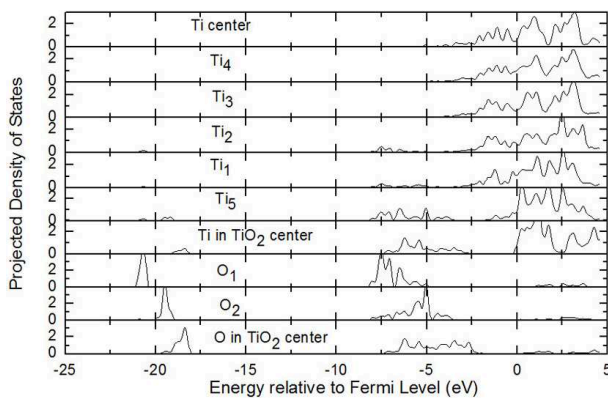


Figure 12: DOS projected onto selected atoms for the single-oxygen interface. The label of the atom is identified in 11.

Atomic, electronic structure of double-oxygen interface using symmetric structure

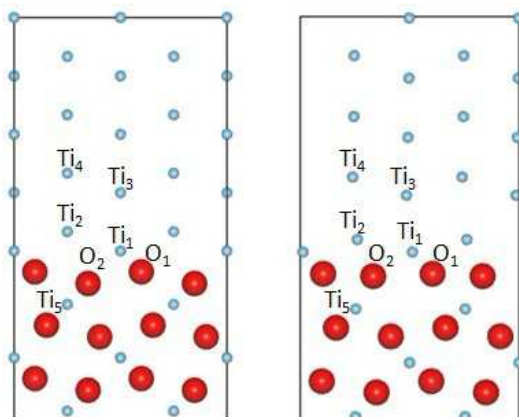


Figure 13: Structure of double-oxygen interface with 'TT' stacking (due to the symmetry, only layers near one interface is shown), viewed along [001] direction of TiO_2 . Left: without atomic relaxation (the equivalent atoms on the boundary are also shown). Right: with atomic relaxation. Red spheres are O atoms, and silver spheres are Ti atoms.

Not surprisingly, 13 is very similar to the 'TT' stacking of Ti-O-O terminated interface obtained using the film-like model. For example, the layer spacing of Ti_1 - Ti_2 is 0.54 \AA , corresponding to 0.55 \AA for Ti_1 - Ti_5 layer in 8; while the spacing of Ti_2 - Ti_3 is 1.90 \AA , very close to the Ti_1 - Ti_2 spacing 1.88 \AA (8). Note that Ti_1 in 13 is in the equivalent position to Ti_5 in 8.

Again the Bader charge (6) and projected DOS (14) agree well with the film-like model (9). Comparing the total density of states (5(c) and 5(e)), only the surface oxygen states in the range from -17.5 eV to -15 eV are absent.

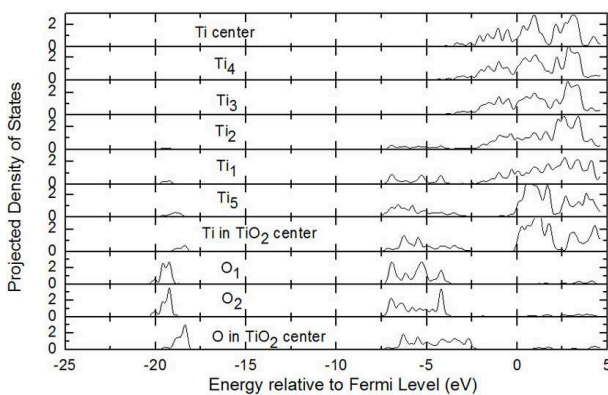


Figure 14: DOS projected onto selected atoms for the double-oxygen interface using symmetric structure. The label of the atom is identified in 13.

Atomic, electronic structure of double-oxygen interface using asymmetric structure

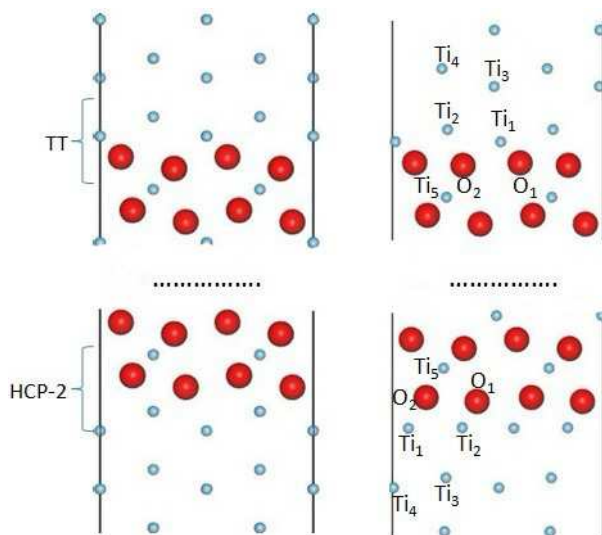


Figure 15: Structure of two double-oxygen interfaces with different stacking sequence, viewed along $[001]$ direction of TiO_2 . The ions in the center of the oxide are omitted. Left: without atomic relaxation (the equivalent atoms on the boundary are also shown). Right: with atomic relaxation. Red spheres are O atoms, and silver spheres are Ti atoms.

As shown in 15, we can consistently reproduce the interface structure with 'TT' stacking (8 and 13) and 'HCP-2' stacking (3) very well in film, symmetric-bulk and asymmetric-bulk calculation. The Bader charges (6) are equivalent to film-like model. The relevant projected DOS compare very well with each other (16 vs 14, and 17 vs 4). Again no surface-atom-induced peak is found in the total DOS figure (5(f)). We can therefore be highly confident that these structures are converged with cell size and not artifacts of the boundary conditions.

CONCLUSION

First-principles calculation is performed to investigate the atomic structure and bonding nature of the $\text{Ti}(10\bar{1}0) // \text{TiO}_2(100)$ interface. A series of tests have been done to verify the settings used in the calculation, by studying the bulk and free surface properties and successful comparison with previous calculation and experimental work.

Two different models are used to simulate the interface. With the film-like model, we consid-

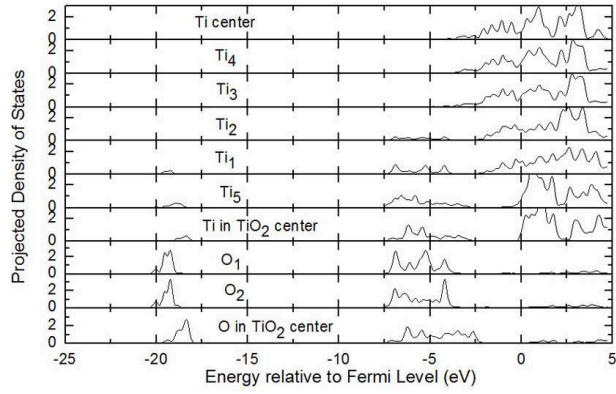


Figure 16: DOS projected onto selected atoms for the 'TT' stacking interface. The label of the atom is identified in 15.

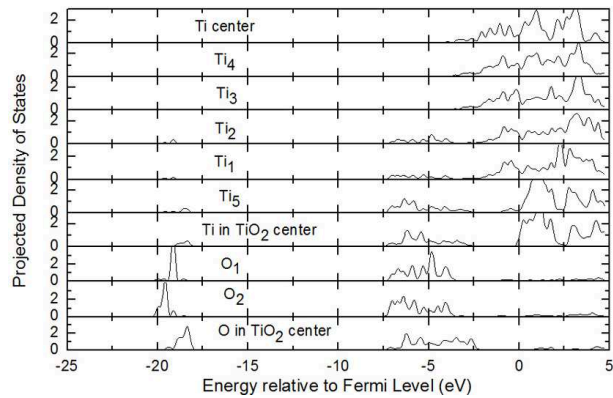


Figure 17: DOS projected onto selected atoms for the 'HCP-2' stacking interface. The label of the atom is identified in 15.

ered three terminations and different stacking sequences. Interfaces compatible with the extension mechanism ('TT' stacking) were constructed for the O-O-Ti and Ti-O-O systems, and we found these geometries quite favored, especially for the Ti-O-O terminated interface. With the bulk-like model, different terminations and stacking sequences were also studied and the interface energy is calculated with no surface energy involved. Except in the one case with anomalous surface reconstruction, agreement between the two models is good.

The relaxations tended to flatten the metallic and ionic surfaces.

Substantial charge transfer in the interface structure is observed, giving interface charges exceeding those in bulk TiO₂ but this is confined to a small region around 5 Å of the interface. As more electrons move to the oxide, the ionic bonding between the interfacial Ti atoms in the metal and the interfacial O in the oxide becomes stronger. These enhanced electrostatic fields at the interface are evidenced by the shift of the low-lying 2s state in the pDOS. More electrons are accepted by the interfacial oxygen ions than oxygen ions in the bulk rutile; this can be easily understood because the electron donors are more abundant in the presence of the metal slab.

From the results of the projected DOS calculation, the picture emerges of metallic bonding changing to ionic bonding over a short region, with enhanced ionic bonding at the interface. In the O-O-Ti and O-Ti-O interfaces, a small covalent component may exist, but for the Ti-O-O interface, no hybridized states are observed on the interfacial Ti of the metal slab, thus no covalent interfacial bonding is formed. Also we notice that new gap states formed in the DOS of interfacial Ti of the oxide. As with structure and Bader charge, the atom-projected DOS is consistent between the two models.

Most notably, the total energy of the slabs containing interfaces is lower than the equivalent numbers of atoms in pure Ti and pure TiO₂. This shows that Ti has strong affinity for oxygen, but at the same time that the oxide is strongly bound to Ti. Combined with the good match of lattice parameters, this helps to explain why the oxide forms such a good protective coating for Ti alloys.

Acknowledgement

The authors would like to acknowledge the support of the European Union Seventh Framework Programme (FP7/2007-2013) under grant agreement No. PITN-GA-2008-211536, project MaM-iNa. The authors also acknowledge the financial support from the MoST of China under Grant No. 2011CB606404.

References

- (1) Lutjering, G., Williams, J. C., Eds. *Titanium*, 2nd ed.; Springer: Germany, 2007.
- (2) Flower, H.; Swann, P. *Acta Metallurgica* **1974**, *22*, 1339 – 1347.
- (3) Kozłowski, M.; Tyler, P.; Smyrl, W.; Atanasoski, R. *Surface Science* **1988**, *194*, 505 – 530.
- (4) Ting, C.-C.; Chen, S.-Y.; Liu, D.-M. *Thin Solid Films* **2002**, *402*, 290 – 295.
- (5) Kumar, S.; Narayanan, T. S.; Raman, S. G. S.; Seshadri, S. *Materials Characterization* **2010**, *61*, 589 – 597.
- (6) Lopez, M.; Jimenez, J.; Gutierrez, A. *Electrochimica Acta* **2003**, *48*, 1395 – 1401.
- (7) Garcia-Alonso, M.; Saldana, L.; Valles, G.; Gonzalez-Carrasco, J.; Gonzalez-Cabrero, J.; Martinez, M.; Gil-Garay, E.; Munuera, L. *Biomaterials* **2003**, *24*, 19 – 26.
- (8) Guleryuz, H.; Cimenoglu, H. *Biomaterials* **2004**, *25*, 3325 – 3333.
- (9) Siegel, D. J.; Hector, L. G.; Adams, J. B. *Phys. Rev. B* **2002**, *65*, 085415.
- (10) Christensen, A.; Carter, E. A. *The Journal of Chemical Physics* **2001**, *114*, 5816–5831.
- (11) Liu, L. M.; Wang, S. Q.; Ye, H. Q. *Surface and Interface Analysis* **2003**, *35*, 835–841.
- (12) Lallet, F.; Olivi-Tran, N.; Lewis, L. J. *Phys. Rev. B* **2009**, *79*, 035413.

- (13) Shang, J.-X.; Guan, K.; Wang, F.-H. *Journal of Physics: Condensed Matter* **2010**, *22*, 085004.
- (14) Kresse, G.; Hafner, J. *Phys. Rev. B* **1993**, *47*, 558–561.
- (15) Kresse, G.; Furthmüller, J. *Phys. Rev. B* **1996**, *54*, 11169–11186.
- (16) G., K.; J., F. *Computational Materials Science* **1996**, *6*, 15–50.
- (17) Blöchl, P. E. *Phys. Rev. B* **1994**, *50*, 17953–17979.
- (18) Perdew, J. P.; Wang, Y. *Phys. Rev. B* **1992**, *46*, 12947–12954.
- (19) Monkhorst, H. J.; Pack, J. D. *Phys. Rev. B* **1976**, *13*, 5188–5192.
- (20) Kittel, C., Ed. *Introduction to Solid State Physics*, 8th ed.; John Wiley and Sons: New York, 2004.
- (21) Burdett, J. K.; Hughbanks, T.; Miller, G. J.; Richardson, J. W.; Smith, J. V. *Journal of the American Chemical Society* **1987**, *109*, 3639–3646.
- (22) GRANT, F. A. *Rev. Mod. Phys.* **1959**, *31*, 646–674.
- (23) III, J. M.; Watson, P. *Surface Science Letters* **1989**, *209*, L105 – L108.
- (24) III, J. M.; Watson, P. *Surface Science* **1989**, *220*, L667 – L670.
- (25) Diebold, U. *Surface Science Reports* **2003**, *48*, 53 – 229.
- (26) Boettger, J. C. *Phys. Rev. B* **1994**, *49*, 16798–16800.
- (27) Erdin, S.; Lin, Y.; Halley, J. W. *Phys. Rev. B* **2005**, *72*, 035405.
- (28) Tyson, W.; Miller, W. *Surface Science* **1977**, *62*, 267 – 276.
- (29) Muscat, J.; Harrison, N. M.; Thornton, G. *Phys. Rev. B* **1999**, *59*, 2320–2326.

- (30) Labat, F.; Baranek, P.; Adamo, C. *Journal of Chemical Theory and Computation* **2008**, *4*, 341–352.
- (31) Perron, H.; Domain, C.; Roques, J.; Drot, R.; Simoni, E.; Catalette, H. *Theoretical Chemistry Accounts: Theory, Computation, and Modeling (Theoretica Chimica Acta)* **2007**, *117*, 565–574, 10.1007/s00214-006-0189-y.
- (32) Zhang, W.; Smith, J. R. *Phys. Rev. Lett.* **2000**, *85*, 3225–3228.
- (33) Iler, J. S.-M.; Kristoffersen, H. H.; Hinnemann, B.; Madsen, G. K. H.; Hammer, B. *The Journal of Chemical Physics* **2010**, *133*, 144708.
- (34) Tang, W.; Sanville, E.; Henkelman, G. *Journal of Physics: Condensed Matter* **2009**, *21*, 084204.
- (35) Paxton, A. T.; Thiên-Nga, L. *Phys. Rev. B* **1998**, *57*, 1579–1584.
- (36) Landa, A.; Söderlind, P.; Ruban, A. V.; Peil, O. E.; Vitos, L. *Phys. Rev. Lett.* **2009**, *103*, 235501.

Graphical TOC Entry

